



OPEN

# Application of drug-induced growth rate inhibition and intracellular drug exposures for comprehensive evaluation of cellular drug sensitivity

Dolonchampa Maji<sup>1,2</sup>, Malerie Wolke<sup>1,2</sup>, Shamim Khaja<sup>1</sup>, John P. Savaryn<sup>1</sup>, John C. Kalvass<sup>1</sup> & Gary J. Jenkins<sup>1</sup>✉

**In vitro cellular assays are indispensable tools for preclinical understanding of therapeutic candidates. Herein, we have outlined methods for robust determination of cellular sensitivities by adapting drug-induced growth-rate inhibition analysis combined with intracellular drug exposure measurements. Using two auristatins as tool molecules, we demonstrate wide variety of cellular response in sensitive versus resistant cancer cells, as well as in a toxicity-relevant cell type. Cellular response analysis generates metrics describing efficacious extracellular concentrations of drug, as well as the phenotype of response—cytotoxic versus cytostatic. Cell associated drug measurements bridge the gap between extracellular drug concentrations and exposure at intracellular sites required for a desired pharmacodynamic response. Such methods can complement rational drug design by providing thorough understanding of the drug mechanism of action, guide mechanistic selection of target indication and inform exposure-response analysis at various stages of drug discovery.**

A crucial part of modern drug development is the fundamental understanding of the exposure-response relationship that drives the pharmacology and toxicology of a therapeutic candidate. This relationship for each drug molecule is defined by the exposure required at the site of action and the time course of exposure, which in turn depends on the biological properties of the target molecule or cellular pathways involved. Recent studies have shown that the inability to achieve adequate drug exposure at the target site of action is one of the primary reasons for attrition during preclinical drug discovery work and ultimate failure in the clinic<sup>1–3</sup>.

Various in vitro tools have been developed for early understanding of drug concentrations required for exerting a desired pharmacodynamic (PD) response in representative biological systems. For example, the “potency” of small molecule oncology drugs is often assessed by obtaining concentration-response curves in a 2D/3D culture of cancer cell lines, from which an  $IC_{50}$  or  $IC_{90}$  value corresponding to the drug concentrations featuring 50% or 90% reduction in signal with respect to untreated control can be derived. The signal measured to generate the curves is a direct or surrogate measurement of the number of viable cells at a treatment endpoint. Amongst others, cellular ATP content is a popular surrogate measurement of the number of viable cells and can be quantified by commercially available assays<sup>4</sup>. However, with such an approach, the resulting drug potency parameter (e.g.,  $IC_{50}$ ) is reported as the nominal concentration added to cell culture media (extracellular concentrations), creating a potential disconnect for intracellular targets. Extracellular concentrations and exposure at the intracellular site of action can vary depending on the drug properties (cellular permeability, interaction with drug metabolizing enzymes, transporters and efflux pumps, binding affinity to non-specific cellular proteins and lipids) and biological target properties (intracellular target concentration, sub-cellular location). The disconnect due to the barriers of intracellular delivery exists for small molecule drugs dosed as themselves or after bioconjugation to a moiety for target mediated intracellular delivery such as in antibody drug conjugates (ADCs) or nanoparticles. In addition, the results of such concentration-response curves has been shown to be sensitive to experimental variables such as cell doubling time, duration of treatment, and specific properties of the endpoint assay, thus confounding the understanding of sensitivity/resistance of a cell type to a particular drug mechanism of action (MoA)<sup>5</sup>.

<sup>1</sup>Quantitative, Translational & ADME Sciences, AbbVie, Inc, North Chicago, IL, USA. <sup>2</sup>Dolonchampa Maji and Malerie Wolke contributed equally to this work. ✉email: gary.jenkins@abbvie.com

There is a need to employ more robust in vitro tools to determine sensitivity of cell/tissue systems to a particular class of drug, as well as to better understand the exposure at the site of action without solely relying on extracellular drug concentrations. In this work, we have attempted to address the gaps stated above. Firstly, to robustly determine cellular sensitivities to drugs, we designed assays and analyzed data by adapting normalized growth-rate inhibition (GR) metrics over traditional metrics of  $IC_{50}$ ,  $EC_{50}$  and  $E_{max}$  parameters (Supplementary Fig. S1)<sup>6</sup>. It has been shown experimentally using a panel of breast cancer cell lines that traditional  $IC_{50}$  and  $E_{max}$  metrics can be highly sensitive to the number of cell division taking place during course of assay<sup>7</sup>. On the contrary, GR-methods quantify drug sensitivity on a per cell division basis. By adopting more uniform cell growth during experiments and utilizing normalized growth rate inhibition-based data analysis, the cellular sensitivity metrics  $GR_{50}$  and  $GR_{max}$  are more robust to experimental variables that impact cell division rates<sup>7–9</sup>. This approach was developed as part of the NIH-LINCS initiative and has been used to explain confounding differences in drug sensitivities across databases and improve preclinical pharmacogenomics<sup>5,7–11</sup>. Secondly, to determine intracellular drug exposures, we have used liquid chromatography tandem mass spectrometry based quantitative bioanalytical tools (LC-MS/MS) capitalizing on the specificity and high-throughput nature of the technique<sup>12,13</sup>. We estimated steady state intracellular concentrations of the drug molecules required to elicit a desired degree of PD response (growth inhibition). A comparison of required intracellular exposures has then been made between the drug molecules and the different cell types studied.

As tool molecules, we chose two microtubule inhibitors (MTIs) from the auristatin family which have been used as payloads for ADCs for target mediated intracellular delivery. Auristatins bind onto the 'peptide site' of  $\beta$ -tubulin in the tubulin heterodimer<sup>14,15</sup>. The mechanism by which they act includes the induction of curved aggregates and inhibition of nucleotide exchange, resulting in inhibition of tubulin polymerization<sup>15–17</sup>. Monomethyl auristatin D (MMAD) and monomethyl auristatin E (MMAE) are synthetic MTIs and have reactive chemical groups for bioconjugation. They have been used as payloads for targeted delivery attached to ADCs. Notably, MMAE has been used in multiple ADCs preclinically for oncology applications and in five out of twelve FDA approved ADCs: Adcetris<sup>®</sup>, Polivy<sup>®</sup> and Padcev<sup>®</sup>, Tivdak<sup>®</sup>, and Aidixi<sup>®</sup>. We characterized these auristatins in a panel of triple negative breast cancer (TNBC) cell lines: MDA-MB-468, HCC1806, HCC1937 and HCC1143. MTIs have been demonstrated to have activity in breast cancer and in TNBC in particular<sup>11,18</sup>. In our experiments, we included the HCC1937 cell line which has demonstrated incomplete growth inhibition in response to paclitaxel and vinorelbine due to functional loss of the tumor suppressor gene BRCA1<sup>19</sup>. In addition, we also used the HCC1143 cell line which demonstrated resistance (high  $IC_{50}$ ) to paclitaxel and eribulin potentially due to upregulation of a cluster of genes in epithelial-to-mesenchymal transition pathway<sup>20</sup>. The comparison between cell lines with different resistance phenotypes will provide information to better understanding of the individual significance of in vitro data metrics generated from the concentration-response data. In addition, we also included liver sinusoidal endothelial cells (LSECs) as a non-cancer cell type to represent a potential toxicologically relevant tissue. In a living system, these cells line the sinusoidal capillary walls of the liver and have direct exposure to therapeutics in circulation. Due to their location and function, they may be particularly sensitive to therapeutics with preferential disposition in the liver tissue. Understanding the relative sensitivity of cancer versus representative toxicity sensitive cells in vitro towards a class of drug molecules (auristatins) can potentially inform better matching of drug MoA to target indication, and ultimately guide the in vivo dosing strategy necessary for the drug to have efficacy in the target tissue while simultaneously avoiding normal tissue toxicity.

## Results

### Permeability, binding, and physicochemical properties of tool molecules

Table 1 summarizes physicochemical parameters for MMAE and MMAD which are key determinants to cellular disposition of the molecules. Both molecules have comparable passive permeability, plasma, and cellular binding. MMAD appears to be a more susceptible substrate of efflux pumps MDR1 and BCRP while also being more lipophilic (higher  $logD$ ) than MMAE. Another key binding parameter is the binding affinity to target tubulin. Literature review found binding affinity ( $K_D$ ) for MMAE-free tubulin binding as 291 nM (fluorescence polarization binding measurement)<sup>15</sup>.  $K_D$  values for MMAD using similar techniques cannot be found.

### Growth rate inhibition (GR) analysis of cellular sensitivity to auristatins

For each drug molecule and cell line, GR analysis was conducted using an online tool (GR calculator)<sup>6</sup> utilizing cell line doubling time and CTG assay viability results at the 3-day treatment endpoint (Supplementary Figs. S2, S3). As outlined in the online tool, GR values at treatment concentration are calculated as follows:

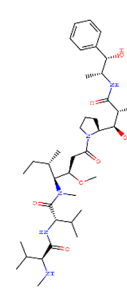
$GR = \frac{c}{k(c)/k(0) - 1}$ , where,  $c$  = concentration;  $k(c)$  = treated growth rate;  $k(0)$  = control growth rate (exponential growth under assay conditions).

Drug potency is defined as media concentration at which the drug produces its pharmacological effect. It is measured by the following metrics:

**GR50** Media Concentration at which  $GR = 0.5$ , or the growth rate of treated cells is inhibited by half relative to untreated cells.

**GEC50** Media concentration required to produce half of maximal response.

GR Analysis demonstrated a range of drug potency as can be anticipated from differential sensitivity of the cells to the drug's MoA (Fig. 1). MTI sensitive cells MDA-MB-468 and HCC1806 cell lines achieved defined  $GR_{50}$  values while MTI resistant HCC1143 and HCC1937 cell lines demonstrated only marginal growth inhibition mostly not reaching  $GR_{50}$  values. An alternate method was used for confirmation of the marginal growth

Drug name & molecular structure	Permeability: $P_{app}$ ÅB in MDCK-MDR1 cells [10e-6 cm/s]	Efflux ratios	Human plasma protein binding (Fu, plasma)	Cellular binding (Fu, cell)	eLogD (pH 7.4)
	0.46 ± 0.13, N = 2	MDRI-MDCK: 50.55 ± 9.97, N = 2 BCRP-MDCK: 4.03 ± 0.62, N = 2	0.26 ± 0.00 n = 3	0.018 n = 1	4.43 ± 0.06, N = 2
	0.40 ± 0.24, N = 2	MDRI-MDCK: 7.23 ± 3.40, N = 3 BCRP-MDCK: 1.30 ± 0.33, N = 3	0.24 ± 0.05 n = 3	0.017 n = 1	3.99 ± 0.09, N = 4

**Table 1.** Permeability, binding, and physicochemical properties of the tool molecules studied. All data represents [mean ± sd, N/n]. N no. of independent experiments, n no. of replicates if a single experiment was performed. *MDR1* multidrug resistance 1 gene expresses P-glycoprotein (P-gp) drug efflux pump, *BCRP* breast cancer resistance protein drug efflux pump.

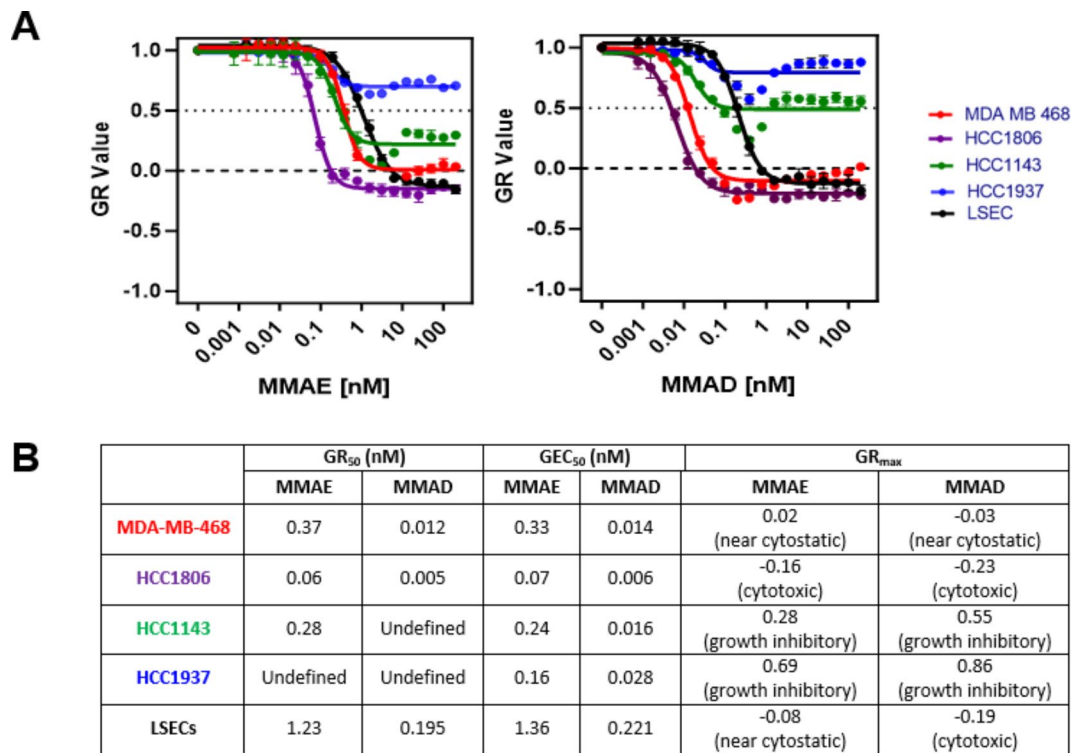


**Fig. 1.** Growth rate (GR) analysis of various auristatin molecules in a variety of breast cancer cell lines and a representative non-cancer cell type. GR values for MMAE and MMAD (A) derived from a CellTiter-Glo with a 3-day treatment end point. Summarized GR parameters demonstrating the range of potency (GR<sub>50</sub>, GEC<sub>50</sub>) and efficacy (GR<sub>max</sub>) across cell lines (B). All data represents mean  $\pm$  sd, for one experiment with  $n=3$  biological replicates.

inhibition in HCC1937 cells and remove possibility of CTG endpoint assay related artifacts. MDA-MB-468 and HCC1937 cell lines were transfected with a fluorescent nuclear marker (nucleic red) and used live cell imaging to longitudinally measure cellular growth behaviors in presence of MMAE. MDA-MB-468 cells growth was completely inhibited at highest doses of MMAE while HCC1937 cells continued to grow with only marginal inhibition (Supplementary Fig. S4). LSECs showed a higher GR<sub>50</sub> values than cancer cell lines, ranging from 3–21x higher for MMAE and 16–39x higher for<sup>21</sup>.

All cells with varying degrees of MTI sensitivity had defined GEC<sub>50</sub> values. Cells with undefined GR<sub>50</sub> (incomplete growth inhibition) had GEC<sub>50</sub> values comparable to those of the cells with defined GR<sub>50</sub> (stronger growth inhibition).

Drug efficacy is defined as the maximum effect that the drug can produce under highest media concentrations evaluated/extrapolated. It is defined with the following metrics:

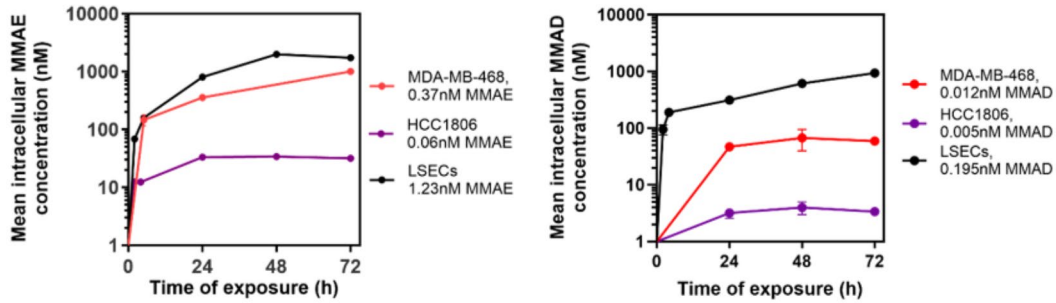
- GR<sub>max</sub> [Range = 1 to -1]: Maximum reduction in growth rate achievable.
- GR<sub>max</sub> > 0: Partial growth inhibition.
- GR<sub>max</sub> = 0: Cytostatic response.
- GR<sub>max</sub> < 0: Cytotoxic response.

A range of drug efficacy was also demonstrated. Maximal growth inhibition phenotype for the MTI sensitive cancer cell MDA-MB-468, HCC1806 as well as LSECs were similar ranging from near cytostatic to mildly cytotoxic behavior. No auristatin exerted a strong cytotoxic response (i.e., GR value approaching -1). This could be related to the MoA of MTIs or auristatins in general. MTI resistant cells HCC1143 and HCC1937 cell lines had GR<sub>max</sub> values indicating incomplete growth inhibition as discussed above.

The corresponding raw CTG endpoint assay results and traditional metrics are calculated and presented in Supplementary Fig. S3. MDA-MB-468 cells demonstrated nearly identical dose response to MMAE in presence and absence of 0.6  $\mu$ M Zosuquidar<sup>22</sup>, a P-gp efflux pump inhibitor (Supplementary Fig. S5).

### Total and unbound cell associated drug concentrations

Cells were treated with 3-day GR<sub>50</sub> drug concentrations for 72 h, and corresponding total cell associated drug concentrations were determined by LC-MS/MS (Supplementary Table T1, Eq. 1). Timepoints earlier than 24 h often had drug concentration below the limit of quantitation. Auristatin molecules reached near-steady state of intracellular drug concentrations within the first 24 h of exposure in most cases (Fig. 2A). Both auristatins demonstrated high cellular partition coefficient (K<sub>p</sub>) in the ~ 400–3500 range (Eq. 2, Fig. 2B). Both were highly

**A****B**

Cell Type	Kp		Kp <sub>uu</sub>		Intracellular Total GR <sub>50</sub> (nM)		Intracellular unbound GR <sub>50</sub> (nM)	
	MMAE	MMAD	MMAE	MMAD	MMAE	MMAD	MMAE	MMAD
<b>MDA-MB-468</b>	1450	3333	32	77	537	40	9.13	0.72
<b>HCC1806</b>	400	400	9	9	24	2	0.41	0.04
<b>LSECs</b>	1164	2503	26	58	1432	488	24.34	8.78

**Fig. 2.** Total and unbound cell associated drug concentrations for auristatins: Mean total cell associated drug concentrations (Eq. 1) versus time profiles for cells treated at respective media GR<sub>50</sub> drug concentrations (A). Data presents mean  $\pm$  sd from  $n=3$  biological replicates in one experiment. A tabulation of cellular partition coefficient (Kp (total) and Kp<sub>uu</sub> (unbound)), and intracellular total and unbound GR<sub>50</sub> drug concentrations (Eqs. 2–5) for each auristatin in the different cell lines/type.

bound in cells with  $F_u$ <sub>cell</sub>  $< 0.02$  (Supplementary Table T2). Unbound cellular partition coefficients (Kp<sub>uu</sub>) were calculated using Eq. 3 and parameters summarized in Supplementary Table T2. Both auristatins showed Kp<sub>uu</sub>  $> 1$  in all cell line/types.

Intracellular Total GR<sub>50</sub> of auristatins were calculated by estimating the near-steady state total cell-associated drug concentrations when cells are treated with GR<sub>50</sub> media drug concentrations (Eq. 4). Intracellular unbound GR<sub>50</sub> were calculated using Eq. 5.

## Discussion

In this work, we have demonstrated methods to estimate intracellular exposures of drug molecules needed to drive a desired PD response. First, in place of traditional drug sensitivity metrics (IC<sub>50</sub>, EC<sub>50</sub>, E<sub>max</sub>), we have employed robust growth rate inhibition (GR) analysis to determine cellular sensitivity to a drug. Then, we have employed LC-MS/MS to quantify cell-associated unconjugated drug molecules and estimated steady state intracellular drug concentrations needed to exert a desired degree of cell growth inhibition. As tool molecules we evaluated two auristatin molecules MMAE and MMAD in target TNBC cell lines and a representative noncancer liver epithelial cell. We have included a comparison of intracellular exposures needed by diseased versus toxicity relevant normal cells as a potential approach to understand selectively drug MoA in a particular indication.

Drug-induced cell growth inhibition analysis (GR analysis) was applied for robust determination of drug potency (GR<sub>50</sub>, GEC<sub>50</sub>) and drug efficacy (GR<sub>max</sub>) parameters (Supplementary Fig. S1). Pre-assay optimization of cell seeding densities ensured all cells were growing exponentially without saturation during assay duration up to 5 days (Supplementary Fig. S2). Cells had at least one cell division which can help minimize impact of cell-cycle status on drug sensitivity outcomes. GR analysis of tool molecules in the cell lines demonstrated a range of potency and efficacy (Fig. 1). Parameters measured at 3-day and 5-day endpoint were comparable (data not shown). Sensitive cells MDA-MB-463, HCC-1806 and LSECs demonstrate defined GR<sub>50</sub> and cytotoxic (GR<sub>max</sub>  $< 0$ ) or near cytostatic response (GR<sub>max</sub> near 0). HCC-1806 demonstrated the highest sensitivity amongst all cell lines with lowest GR<sub>50</sub> and cytotoxic activity at the highest dose evaluated for both auristatins. Diminished sensitivity to auristatin MoA in HCC-1143 and HCC-1937 cells is primarily demonstrated by undefined GR<sub>50</sub> and partial growth inhibitory response (GR<sub>max</sub>  $> 0$ ) while GEC<sub>50</sub> values were comparable to other cell lines. This underlies the significance and complementarity of individual parameters derived from a dose response assay. The resistance of cell lines may not always manifest as relatively higher GR<sub>50</sub>, IC<sub>50</sub> but as only incomplete growth inhibitory effects at highest dose evaluated. The underlying CTG endpoint assay data was also analyzed to give the corresponding IC<sub>50</sub>, EC<sub>50</sub> and E<sub>max</sub> values are shown in (Supplementary Fig. S3). By conducting cellular experiments following optimized cell seeding density and assay duration, we minimized the potential impact of cell growth rate and assay conditions on the assay results. Under these optimized assay conditions, GR<sub>50</sub> values were like IC<sub>50</sub> values, GEC<sub>50</sub> values were like EC<sub>50</sub>. Higher E<sub>max</sub> values were related to stronger efficacy, i.e., more cytotoxicity. In general, the overall trends in GR-metrics were comparable for MMAE and MMAD in each cell line/type, and it is anticipated that drugs with varied MoA will result in variable GR-metrics in the same

cell line<sup>11</sup>. MMAD consistently demonstrated lower (6-31x) GR<sub>50</sub> than MMAE. Hence, drug potency based on media drug concentration measurements indicated MMAD is more potent than MMAE.

Eflux pumps are overexpressed and are known to contribute to the drug resistance mechanism of TNBC<sup>23</sup>. Since both auristatins are strong substrates of eflux pump P-gp, we evaluated the potential role of drug eflux pumps in determining cellular sensitivity to auristatins. As representative cell line, we chose MDA-MB-468 which is known to have overexpression of P-gp<sup>21,24</sup>. However, we did not find any appreciable change in dose response upon P-gp inhibition, indicating insignificant role of P-gp in determining disposition of MAME in this cell line. Subsequently no further investigation was conducted using eflux pump inhibitors.

GR-analysis resulted in drug potency (GR<sub>50</sub>) values as extracellular drug concentrations, however since the target tubulin protein is intracellular, a more representative measurement of drug exposure at site of action would be intracellular drug concentration. To further understand if the extracellular concentration-based differences in auristatin drug potency translated to intracellular exposures, we treated cell line/type at their respective GR<sub>50</sub> drug concentration and quantified resulting intracellular unconjugated drug concentration using LC-MS/MS analysis (Fig. 2A). This time course data was used to calculate cellular partition coefficient K<sub>p</sub>, unbound cellular partition coefficient K<sub>p<sub>uu</sub></sub> (Eqs. 2, 3, Fig. 2B). Both auristatins had high cellular partitioning, K<sub>p</sub>, in the 400–3500 range (Fig. 2B). It can be expected as MMAE and MMAD are lipophilic compounds (Table 1), and exhibit moderate plasma protein binding (Fu plasma, Table 1) but high cellular binding (Fu cell, Table 1) likely owing to the abundance of intracellular target tubulin and high non-specific binding to cellular lipids. High cellular retention of MMAE indicating highly bound nature in cells has been previously reported<sup>25</sup>. Herein, we have assumed that Fu, cell experimentally measured using cell homogenate translates to cellular binding under physiological conditions. It is possible that the concentration of drug used in Fu assay may have been high where specific binding to tubulin was saturated, resulting in an over-estimation of cellular binding. Both auristatins exhibited high intracellular partition coefficient K<sub>p<sub>uu</sub></sub>>1. This indicates when the cells are exposed to the GR<sub>50</sub> drug concentrations in media, unbound drug accumulated at a higher concentration relative to media, suggesting potential role of active drug transporters in the cellular accumulation and retention of MMAE and MMAD.

Intracellular GR<sub>50</sub> concentrations were calculated by estimating the near-steady concentrations of total cell associated drug concentration at GR<sub>50</sub> treatment (Eq. 4, Fig. 2B). Intracellular unbound GR<sub>50</sub> were obtained by correcting total cell associated concentration with cellular binding (Eq. 5, Fig. 2B). In general, intracellular total and unbound concentrations GR<sub>50</sub> followed the same trend as media GR<sub>50</sub> drug concentrations. MMAE had higher intracellular total and unbound GR<sub>50</sub> than MMAD, suggesting need for higher compound concentration to drive the same pharmacodynamic response than MMAD. In summary, MMAE and MMAD possess similar permeability, binding and physicochemical properties and it resulted in similar cellular disposition, hence media GR<sub>50</sub> translated well into their intracellular measurements. MMAD is a more potent compound when used as small molecule drug and is expected to be more potent when delivered using targeted methods such as ADCs. Better target binding resulting in superior intracellular potency is demonstrated in literature by cell impermeable monomethyl auristatin F (MMAF)<sup>15</sup>. MMAF has ~5x better tubulin binding affinity than MMAE in a cell free system<sup>15</sup> but demonstrates reduced potency (higher media IC<sub>50</sub>) in cells as it is unable to diffuse across the plasma membrane<sup>26</sup>. However, antibody conjugates of MMAF can be very potent in cells partly explained and by its high intracellular tubulin binding<sup>26,27</sup>. This example also illustrates two molecules with the same MoA may have different media versus intracellular potency owing to difference in cellular permeability, hence the importance of intracellular drug concentration measurements. Our literature review did not find tubulin binding affinity for tool molecule MMAD; hence explanation of intracellular potency differences between MMAE and MMAD based on tubulin binding affinity could not be included here.

In this work, we have compared two similar auristatin molecules across TNBC cancer cell lines as diseased target cells and a non-cancer cell type, LSEC, as a representative of toxicity-sensitive cells. This has allowed us to calculate an effective in vitro therapeutic index (TI) as the ratio of intracellular GR<sub>50</sub> in LSEC to that in the cancer cell lines. This surrogate measurement indicates the relative sensitivity of the diseased versus toxicity sensitive normal cells to individual drug MoA. Such surrogate measurements can enable rank ordering different drugs/MoAs by their ability to differentiate between diseased versus normal tissue for a particular disease indication. Emerging understanding of toxicity of targeted therapeutics such as ADCs has enabled identification of cell lines within a toxicity relevant organ or tissue. For example, mannose receptor expressing LSECs are implicated in target independent uptake of ADCs resulting in off-target hepatic toxicity<sup>28</sup>. Hence, in vitro assays using cell culture of appropriate cell types can be used to calculate in vitro TI as an early read out of the intrinsic ability of drugs to differentiate between diseased and normal cells, tissue or organs. Herein, we have provided interpretation of in vitro TI using limited data on two remarkably similar molecules. We anticipate more differentiation in TI indices when drugs from different MoA classes are used. Our results show both auristatins have a positive in vitro TI: MMAE: 3–60x; MMAD: 12–244 (Supplementary Table T3). Hence, the tested TNBC cell lines were selectively more sensitive to both auristatins, and MMAD may better differentiate between TNBC and representative normal cells. By extension, an ADC designed for TNBC indication and potential toxicities in liver tissue could utilize an auristatin payload to provide selective protection to sensitive normal tissue. On the other hand, when comparing cellular efficacy parameter GR<sub>max</sub> no clear trend was observed differentiating cancer versus LSECs (Supplementary Table T3). At the highest dose evaluated, all auristatins elicited moderately growth inhibitory to moderately cytotoxic behavior. This result highlights if overdosed, the auristatins may lose the ability to provide selective sensitivity to cancer cells and cause equal damage to both targeted diseased and toxicity sensitive tissue.

By virtue of using intracellular measurements for calculating in vitro TI, as opposed to media measurements, we were able to compare the inherent cellular sensitivities to the drugs when delivered by intracellularly targeted platform such as ADCs. Using an index that can compare diseased versus normal tissue provides added benefit

over and above using GR-metrics to select disease indication by virtue of high drug efficacy and potency in diseased cells only<sup>11</sup>.

While applying the GR methods, we have assumed the resulting growth rates in presence of drugs are approximately exponential and conducted GR analysis based on the 3-day assay endpoint. We have utilized an endpoint assay dependent on quantification of cellular ATP (CTG Assay 2.0, Promega). By virtue of being an endpoint assay, there is a risk of losing information by not analyzing early and intermediate timepoints. In addition, surrogate measurements of cell viability such as by ATP content or MTS assay (quantifies NADPH-dependent dehydrogenase enzymes) may not allow accurate determination of cellular sensitivity due to discrepant measurements of cell count<sup>29</sup>. They have been shown to often underestimate drug potency and efficacy. To avoid these issues, instead of relying on a surrogate endpoint assay one may enable accurate measurements of cell counts during the multiday assay. One way to do this is by transfecting the cell line with a fluorescent nuclear marker and using imaging for counting cell nuclei in high throughout plate base damaging systems (Fig. S4). Time-dependent cell count information can be used for time-dependent GR-analysis for in depth information on diverse mechanisms of drug sensitivity and resistance<sup>7</sup>. In addition, fluorescence markers for specific phenotype such as apoptosis, senescence or cell death can also be used.

While the methods are straightforward, the output data is sensitive to accurate measurement of number of cells in the LC-MS/MS samples and mean cellular diameter. As good practice, we counted cells and measured diameters only after treatment endpoint and all wash steps were completed and samples were ready for LC-MS/MS analysis. All cells evaluated were adherent cells and required trypsinization post treatment endpoint, which may lead to loss of cell-associated drug due to passive permeability and active drug transporter/efflux pumps activity. To further minimize such loss, one can consider culturing adherent cells in suspension mode and bypassing post-treatment trypsinization for such experiments. For all processes post trypsinization, we maintained cells and equipment at 4 °C or on ice. Another alternative is to extract cellular drug from an adherent monolayer. However, this may increase risk of organic solvent evaporation during extraction, as well as extraction of compound absorbed/adsorbed non-specifically into the cell culture plasticware<sup>30</sup>. We used GR<sub>50</sub> media doses for quantification of intracellular exposures which resulted in growth inhibition. However, at higher doses the drugs can exert a dominant cytotoxic response which will result in loss of representative cells, hence a potential loss of representative data from LC-MS/MS quantification.

The methods described in this work provide ways to better understand exposures at the intracellular site of action required to elicit a PD response. Application of GR-analysis enables robust determination of cellular sensitivity by removing confounding experimental variables such as cell seeding density while informing on both drug potency (GR<sub>50</sub>, GEC<sub>50</sub>) and phenotype of response at the highest doses evaluated (GR<sub>max</sub>). In addition, using a surrogate measurement such as in vitro therapeutic index that compares diseased versus normal cells provides added benefit over using drug sensitivity in diseased cells only. In early drug discovery stages, such methods can complement rational drug design and match target indication to drug MoA, especially for intracellularly targeted delivery platforms. In late-stage drug discovery and development, similar methods can validate drug MoA and inform mechanistic exposure-response analysis to project efficacious doses and dosing strategies.

## Methods

### Physicochemical properties of tool molecules

Data summarized in Table 1 were generated using previously described methods<sup>31–34</sup>.

### Cell culture

MDA-MB-468, HCC1806, HCC-1937 and HCC-1143 cell lines were obtained from ATCC or the AbbVie Biorepository. MDA-MB-468 and HCC1806 cells were grown in Dulbecco's Minimum Essential Medium (DMEM) containing 10% fetal bovine serum (FBS). HCC1143 and HCC1937 cells were cultured in Roswell Park Memorial Institute medium (RPMI) containing 10% FBS. Primary human liver sinusoidal endothelial cells (LSECs) were obtained from Cell Systems and cultured as recommended by the vendor. All cell lines were grown under standard conditions (37 °C with 5% CO<sub>2</sub>).

### Growth curves for optimal seeding densities

Optimal seeding density for log-phase growth under assay duration was determined for each cell type by plating 500–7500 cells per 200µL media in a 96 well plate (surface area = 0.32cm<sup>2</sup> /well) (Fig. S3). Cells were seeded in triplicate and allowed to adhere to the plates for ~ 24 h then bright field images of cell growth were captured (every 2–6 h) by an Incucyte Zoom Live-Cell Analysis System (Essen Bioscience) for 5 days. Corresponding bright field confluence area was obtained by Incucyte image analysis software and plotted for visualizing the seeding density dependent growth properties using Prism (GraphPad). Cell doubling time was determined by fitting longitudinal confluence data using exponential cell growth equation on Prism.

### CellTiter-glo (CTG) assay

For generating concentration-response curves, cells were seeded at the optimal seeding were allowed to incubate at 37 °C with 5% CO<sub>2</sub> for 24 h to allow cells to adhere prior to treatment. Cells were treated with 0–200nM of MMAE or MMAD continuously for 3 and 5 days. At the end of treatment, CellTiter-Glo 2.0 reagent was used according to manufacture instructions and viability results read with an EnSpire Multimode Plate Reader. For all reported data in these studies, the 3-day endpoint was used.

For evaluating effect of P-gp inhibition on MDA-MB-468 cells, CTG assays were conducted in presence and absence of 0.6 µM Zosuquidar [P-gp inhibition Ki = 0.06 µM] in parallel. Comparison of auristatin free cells in presence and absence of Zosuquidar confirmed the P-gp inhibitor by itself did not have undesired effect on cell growth.

### Drug-induced growth rate inhibition (GR) analysis

For each drug molecule and cell line/type, GR analysis was conducted using an online tool available to the public<sup>6</sup>. Cell line doubling time was used to calculate number of cell divisions under experimental conditions. CTG assay viability results at the 3-day treatment endpoint were used as a surrogate measurement of number of viable cells. Representative  $IC_{50}$ ,  $EC_{50}$ ,  $E_{max}$  was calculated on Prism [GraphPad].

### Measurement and calculations related to intracellular drug concentrations

For each drug molecule, cell lines with a defined  $GR_{50}$  value (i.e., media drug concentration at which GR value = 0.5 non-treated control GR) were chosen to further understand intracellular exposures. Cells were plated at the previously described seeding densities, scaled up to include enough cells required for LC-MS/MS sensitivity and treated with drug at their respective  $GR_{50}$  concentrations. Treatment media was removed from cells at 2, 4 or 5, 24, 48 and 72 h, cells were washed twice with PBS, trypsinized and resuspended into a single cell suspension. Triplicate cell samples (25  $\mu$ L each) were then taken for LC-MS/MS analysis and the remainder was used for measuring cell number, diameter, and viability. Media samples from each timepoint were also taken for LC-MS/MS analysis.

Standard curves of MMAE and MMAD were created in DMSO using a Hamilton Automated Liquid Handling Microlab STAR. All samples and standards were volume and matrix matched with untreated cells and DMSO prior to extraction by protein precipitation. Samples and standards were processed with protein precipitation using 100  $\mu$ L of 95:5 acetonitrile: methanol containing internal standards, vortexed at 1600 rpm for 1 min, followed by centrifugation at 3202xg for 5 min prior to analysis with LC-MS/MS.

LC-MS/MS analysis was performed with a Sciex 6500 Triple Quad mass spectrometer using multiple reaction monitoring (MRM) coupled to an Agilent 1290 LC system with a CTC PAL autosampler. A Phenomenex Kinetex C18 Reversed Phase Column 30  $\times$  2.1 mm with 5  $\mu$ m particle size was used with a 1-minute elution gradient. Mobile Phase A was composed of high-performance liquid chromatography (HPLC) grade water with 0.1% formic acid. Mobile phase B consisted of HPLC grade acetonitrile with 0.1% formic acid. The MRM transitions were: MMAE  $m/z$  718.6  $\rightarrow$  685.5, MMAD  $m/z$  771.6  $\rightarrow$  188.1.

The sample was initially held at 95% mobile phase A and 5% mobile phase B for 0.2 min to ensure retention and sufficient clean up. The gradient was ramped to 95% mobile phase B over the following 0.6 min, where it was held for an additional 0.2 min. The gradient was then brought back to initial conditions for 0.02 min. The total flow rate was held at 1500  $\mu$ L/min. The analyte and internal standard peak areas were determined using Sciex Analyst™ 1.7 software. The analyte concentrations of each sample were calculated by least squares regression analysis of the peak area ratio (analyte/ internal standard) of the standards matrix matched with cells versus concentration.

The standard curves were fit using a quadratic 1/X weighted regression and met a minimum correlation coefficient value of 0.98; the lower limit of quantitation (LLOQ) is defined as the lowest standard curve point for a given species with a signal to noise ratio greater than three.

For each drug in a cell line, parameters reported in Fig. 2B were calculated as follows:

$$\text{Mean Intracellular Drug Concentration } [nM] = \frac{\text{Mean cell associated drug per live cell (nanomoles)}}{\text{Mean single live cell volume} = \frac{4}{3} * \pi * r^3 \text{ (liters)}} \quad (1)$$

where,  $r$  = Mean radius of a single liver cell as measured from experimental cell samples.

$$\text{Partition coefficient } [Kp] = \frac{AUC0 - 72h \text{ [Mean intracellular drug concentration vs. time]}}{AUC0 - 72h \text{ [Measured media drug concentration vs. time]}} \quad (2)$$

$$\text{Unbound partition coefficient } [Kpuu] = \frac{\text{Partition coefficient } [Kp] * Fu, \text{ cell}}{Fu, \text{ media}} \quad (3)$$

where,  $Fu_{\text{media}} \approx Fu_{10\% \text{ plasma}}$  was derived from  $Fu$ , plasma values by adjusting for a dilution factor of 10. This was done since cells were incubated in culture media with 10% fetal bovine serum.

For cases where the media concentrations were too low to be accurately quantifiable, a constant media concentration equal to that dosed initially was assumed throughout the time course. Thereby, denominator for Eq. 2 was estimated to be [Media  $GR_{50} * 72$  hours].

Intracellular total and unbound  $GR_{50}$  were calculated using following equations as the steady state intracellular concentration when cells are treated at  $GR_{50}$  media concentrations.

$$\text{Intracellular GR50 } [nM] = \text{Media GR50} * Kp \quad (4)$$

$$\text{Intracellular unbound GR50 } [nM] = \text{Intracellular GR50 } [nM] * Fu, \text{ cell} \quad (5)$$

### Measurement of fraction unbound in cells (Fu, cell)

Flux dialysis experiment was conducted to determine compounds undiluted fraction ( $F_u$ ) using method described previously<sup>34</sup>. Briefly, in accordance with the manufacturer's recommendations, MWCO 12–14 kDa cellulose dialysis membrane strips (HTDialysis, Cat. No. 1101) were prepared and placed into an HTDialysis 96b apparatus (HTDialysis, Cat. No. 1006). MDA-MB-468 cell pellet (~ 100 million cells) was diluted to 20-fold in 1X PBS pH 7.4 (ThermoFisher #14190-144), to homogenize cells were sonicated for 2 pulses of 20 s, 60% intensity resting in between on ice for 1 min. Cell homogenate was then supplemented with 10  $\mu$ M final concentration of sodium azide to prevent microbial growth over the long incubation period. Cell homogenate containing 1

$\mu\text{M}$  of test compound (donor matrix) was dialyzed against compound-free cell homogenate (receiver matrix) in the HTDialysis apparatus at 37 °C with 5% CO<sub>2</sub> and shaking at 160 RPM for up to 120 h. Aliquots (10  $\mu\text{L}$  each) of both donor and receiver matrix were taken at 0, 0.25, 0.5, 2, 4, 24, 48, 72, 96 and 120 h and stored at –20 °C until LC-MS/MS analysis. Standard curves were prepared in DMSO. All samples and standards were volume and matrix matched with cell homogenate, quenched with 150  $\mu\text{L}$  of acetonitrile/methanol (95/5, v/v) containing 50nM carbutamide internal standard, vortexed on VWR VX2500 multitube vortex for 2 min with a speed setting of 5. Samples are centrifuged at 1800xg for 15 min at 4 °C.

For compound quantification using HPLC-MS/MS, 5 $\mu\text{l}$  supernatant was injected onto a Waters Xbridge C8 column using CTC PAL autosampler connected to an Agilent 1290 HPLC and an Sciex API 6500+ with a turbo spray ion source. Mobile Phase A was composed of high-performance liquid chromatography (HPLC) grade water with 0.1% formic acid. Mobile phase B consisted of HPLC grade acetonitrile with 0.1% formic acid. The sample was initially held at 95% of 0.1% formic acid (mobile phase A) and 5% of 0.1% formic acid in acetonitrile (mobile phase B) for 0.05 min. The gradient was ramped to 2% mobile phase A over the following 0.3 min, where it was held for an additional 0.7 min. The gradient was then brought back to initial conditions for 0.8 min. The total flow rate was held at 800  $\mu\text{L}/\text{min}$ .

The MRM transitions were: MMAE *m/z* 718.6 / 152.1, MMAD *m/z* 771.6 / 188.1. The analyte and internal standard peak areas were determined using Sciex Analyst™ 1.7 software. The analyte concentrations of each sample were calculated by least squares regression analysis of the peak area ratio (analyte/ internal standard) of the standards matrix matched with cells versus concentration.

The standard curves were fit using a quadratic 1/X weighted regression and met a minimum correlation coefficient value of 0.98; the lower limit of quantitation (LLOQ) is defined as the lowest standard curve point for a given species with a signal to noise ratio greater than 3.

% Recovery and receiver/donor ratio of each compound were calculated using following equations described previously<sup>34</sup>. The rate of flux is calculated by plotting the ratio of receiver/donor against time. The slope was calculated on Prism (GraphPad) using non-linear regression with 1/y weighting, the slope of the line (flux rate, 1/h) was converted to unbound fraction using the flux scaling factor. The flux scaling factor is the measured fu/flux rate that was determined using a set of reference compounds.

## Data availability

Data sets generated during the current study are available from the corresponding author on reasonable request. All data is property of AbbVie Inc.

Received: 29 May 2024; Accepted: 15 January 2025

Published online: 11 February 2025

## References

1. Arrowsmith, J. Phase II failures: 2008–2010. *Nat. Rev. Drug Discov.* **10** (5). (2011). Gale OneFile: Health and Medicine, link.gale.com/apps/doc/A256280550/HRCA?
2. Morgan, P. et al. Can the flow of medicines be improved? Fundamental pharmacokinetic and pharmacological principles toward improving phase II survival. *Drug Discov. Today* **17** (9–10), 419–424 (2012).
3. Mateus, A. et al. Prediction of intracellular exposure bridges the gap between target-and cell-based drug discovery. *Proc. Natl. Acad. Sci.* **114** (30), E6231–E6239 (2017).
4. [https://www.promega.com/products/cell-health-assays/cell-viability-and-cytotoxicity-assays/celltiter\\_glo-2\\_0-assay/?catNum=G9241#protocols](https://www.promega.com/products/cell-health-assays/cell-viability-and-cytotoxicity-assays/celltiter_glo-2_0-assay/?catNum=G9241#protocols)
5. Hafner, M., Niepel, M. & Sorger, P. K. Alternative drug sensitivity metrics improve preclinical cancer pharmacogenomics. *Nat. Biotechnol.* **35** (6), 500–502 (2017).
6. Clark, N. A. et al. GRcalculator: an online tool for calculating and mining dose–response data. *BMC Cancer* **17** (1), 1–11 (2017).
7. Hafner, M. et al. Growth rate inhibition metrics correct for confounders in measuring sensitivity to cancer drugs. *Nat. Methods* **13** (6), 521–527 (2016).
8. Hafner, M. et al. Designing drug-response experiments and quantifying their results. *Curr. Protoc. Chem. Biol.* **9** (2), 96–116 (2017).
9. Niepel, M. et al. Measuring cancer drug sensitivity and resistance in cultured cells. *Curr. Protoc. Chem. Biol.* **9** (2), 55–74 (2017).
10. Fallahi-Sichani, M. et al. Metrics other than potency reveal systematic variation in responses to cancer drugs. *Nat. Chem. Biol.* **9** (11), 708–714 (2013).
11. Hafner, M. et al. Quantification of sensitivity and resistance of breast cancer cell lines to anti-cancer drugs using GR metrics. *Sci. Data* **4** (1), 1–9 (2017).
12. Bhat, J. et al. LC-MS based assay to measure intracellular compound levels in *Mycobacterium smegmatis*: linking compound levels to cellular potency. *J. Microbiol. Methods* **94** (2), 152–158 (2013).
13. Wu, C. et al. Intracellular accumulation as an indicator of cytotoxicity to screen hepatotoxic components of *Chelidonium majus* L. by LC-MS/MS. *Molecules* **24** (13), 2410 (2019).
14. Bai, R., Pettit, G. R. & Hamel, E. Dolastatin 10, a powerful cytostatic peptide derived from a marine animal. Inhibition of tubulin polymerization mediated through the vinca alkaloid binding domain. *Biochem. Pharmacol.* **39** (12), 1941–1949 (1990).
15. Waight, A. B. et al. Structural basis of microtubule destabilization by potent auristatin anti-mitotics. *PLoS One* **11** (8), e0160890 (2016).
16. Bai, R. L., Pettit, G. R. & Hamel, E. Binding of dolastatin 10 to tubulin at a distinct site for peptide antimitotic agents near the exchangeable nucleotide and vinca alkaloid sites. *J. Biol. Chem.* **265** (28), 17141–17149 (1990).
17. Bai, R. et al. Interaction of dolastatin 10 with tubulin: induction of aggregation and binding and dissociation reactions. *Mol. Pharmacol.* **47** (5), 965–976 (1995).
18. Nagayama, A. et al. Novel antibody-drug conjugates for triple negative breast cancer. *Ther. Adv. Med. Oncol.* **12**, 1758835920915980 (2020).
19. Quinn, J. E. et al. BRCA1 functions as a differential modulator of chemotherapy-induced apoptosis. *Cancer Res.* **63** (19), 6221–6228 (2003).
20. Dezso, Z. et al. Gene expression profiling reveals epithelial mesenchymal transition (EMT) genes can selectively differentiate eribulin sensitive breast cancer cells. *PLoS One* **9** (8), e106131 (2014).

21. Zhao, Y. et al. Eradication of cancer stem cells in triple negative breast cancer using doxorubicin/pluronic polymeric micelles. *Nanomedicine* **24**, 102124 (2020).
22. Dantzig, A. H. et al. Reversal of P-glycoprotein-mediated multidrug resistance by a potent cyclopropylbenzosuberane modulator, LY335979. *Cancer Res.* **56** (18), 4171–4179 (1996).
23. Abd El-Aziz, Y. S. et al. Role of ABCB1 in mediating chemoresistance of triple-negative breast cancers. *Biosci. Rep.* **41** (2). (2021).
24. Deshmukh, R. R. et al. P-glycoprotein inhibition sensitizes human breast cancer cells to proteasome inhibitors. *J. Cell. Biochem.* **118** (5), 1239–1248 (2017).
25. Singh, A. P. & Shah, D. K. Measurement and mathematical characterization of cell-level pharmacokinetics of antibody-drug conjugates: a case study with trastuzumab-vc-MMAE. *Drug Metab. Dispos.* **45** (11), 1120–1132 (2017).
26. Li, F. et al. Intracellular released payload influences potency and bystander-killing effects of antibody-drug conjugates in preclinical models. *Cancer Res.* **76** (9), 2710–2719 (2016).
27. Doronina, S. O. et al. Enhanced activity of monomethylauristatin F through monoclonal antibody delivery: effects of linker technology on efficacy and toxicity. *Bioconjug. Chem.* **17** (1), 114–124 (2006).
28. Nguyen, T. D., Bordeau, B. M. & Balthasar, J. P. Mechanisms of ADC toxicity and strategies to increase ADC tolerability. *Cancers (Basel)* **15** (3), 713. <https://doi.org/10.3390/cancers15030713> (2023).
29. Chan, G. K. et al. A simple high-content cell cycle assay reveals frequent discrepancies between cell number and ATP and MTS proliferation assays. *PLoS One* **8** (5), e63583 (2013).
30. Palmgrén, J. J. et al. Drug adsorption to plastic containers and retention of drugs in cultured cells under in vitro conditions. *Eur. J. Pharm. Biopharm.* **64** (3), 369–378 (2006).
31. Muschong, P. et al. Improvement of workflows and assay reproducibility by the introduction of assay-ready culturing of MDCK cells for transport studies. *Pharm. Res.* **40** (5), 1259–1270 (2023).
32. Lombardo, F. et al. ElogD(oct): a tool for lipophilicity determination in drug discovery. 2. Basic and neutral compounds. *J. Med. Chem.* **44** (15), 2490–2497 (2001).
33. Wang, Y. T. et al. Integrity and efficiency: AbbVie's journey of building an integrated nonregulated bioanalytical laboratory. *Bioanalysis* **15** (3), 161–176 (2023).
34. Kalvass, J. C. et al. Mathematical and experimental validation of flux dialysis method: an improved approach to measure unbound fraction for compounds with high protein binding and other challenging properties. *Drug Metab. Dispos.* **46** (4), 458–469 (2018).

## Acknowledgements

We thank Prathap Mahalingaiah, Shannon Nottoli and Edit Tarcsa for the constructive scientific discussions and guidance. We thank Sylvia Hellwig, Juliane Hoeckels-Messemer, Daniel Metzger, and Manuel Weinheimer for generating permeability and efflux data presented in (Table 1). We thank Jenna Henning and Paul R Lesniak for generating Fu, plasma data presented in (Table 1).

## Author contributions

DM, GJ designed the study. DM, MLW, SK carried out the experimental work and analyzed the data. DM, MLW wrote the manuscript and contributed equally. All authors provided guidance while writing, edited, and approved the final manuscript.

## Funding

All authors are employees of AbbVie and may own AbbVie stock. The design, study conduct, and financial support for this research were provided by AbbVie. AbbVie participated in the interpretation of data, review, and approval of the publication. The manuscript contains no proprietary AbbVie data.

## Declarations

### Competing interests

The authors declare no competing interests.

### Additional information

**Supplementary Information** The online version contains supplementary material available at <https://doi.org/10.1038/s41598-025-86919-7>.

**Correspondence** and requests for materials should be addressed to G.J.J.

**Reprints and permissions information** is available at [www.nature.com/reprints](http://www.nature.com/reprints).

**Publisher's note** Springer Nature remains neutral with regard to jurisdictional claims in published maps and institutional affiliations.

**Open Access** This article is licensed under a Creative Commons Attribution-NonCommercial-NoDerivatives 4.0 International License, which permits any non-commercial use, sharing, distribution and reproduction in any medium or format, as long as you give appropriate credit to the original author(s) and the source, provide a link to the Creative Commons licence, and indicate if you modified the licensed material. You do not have permission under this licence to share adapted material derived from this article or parts of it. The images or other third party material in this article are included in the article's Creative Commons licence, unless indicated otherwise in a credit line to the material. If material is not included in the article's Creative Commons licence and your intended use is not permitted by statutory regulation or exceeds the permitted use, you will need to obtain permission directly from the copyright holder. To view a copy of this licence, visit <http://creativecommons.org/licenses/by-nc-nd/4.0/>.

© The Author(s) 2025